ISBN: 978-3-95450-219-6 ISSN: 2226-0366 doi: 10.18429/JACoW-LINAC2024-THPB096

CHROMATIC INDEX TO FIND A WORKING POINT FOR A 4TH GENERATION SYNCHROTRON LIGHT SOURCE

E. Sánchez*,[1], A. Flores-Tlalpa[2], J. Hernández-Cobos[1], M. Moreno[3], A. Antillón[1]
[1]Instituto de Ciencias Físicas, Universidad Nacional Autónoma de México, Morelos, México
[2]Departamento de Bioingeniería y Ciencias, Tecnológico de Monterrey, Puebla, México
[3]Instituto de Física, Universidad Nacional Autónoma de México, Cd. de México, México

Abstract

Optimizing the electron dynamics generated by MBA cells involves adjusting a large number of parameters while meeting complex constraints. These optimizations are typically performed using methods that involve calculating standard nonlinear functions, such as dynamic aperture. These methods are often computationally expensive. Recently, a quasi-invariant surface technique for optimizing nonlinear electron dynamics in storage rings has been reported. Building on this approach, a framework for optimizing the linear parameters of a lattice without the need for particle tracking, or similar nonlinear calculations, is proposed. This framework enables the definition of the distorted chromatic index $\zeta_{D,\delta}$, a valuable function for analyzing and tuning a cell to identify a suitable working point for a machine. As an example, these techniques are applied to identify a working point for a ring model based on a 7BA cell, which comprises 20 cells and has a circumference of approximately 490 meters. After conducting nonlinear optimization, this approach achieves stable horizontal amplitudes exceeding 5 mm for momentum deviations between −3% and 3%.

INTRODUCTION

Fourth-generation synchrotron light sources heavily rely on MBA cells. However, controlling the complex electron dynamics generated by these magnetic structures presents significant challenges. For instance, adjusting numerous parameters and meeting stringent constraints require sophisticated and computationally intensive tools. To address these challenges, various techniques are employed, including global analyses of storage ring lattices [1], global optimizations of storage ring lattices [2], frequency map analysis [3], and the calculation of dynamic and momentum apertures using particle tracking [4, 5]. Additionally, methods such as minimization of resonance driving terms [6–8] and hybrid or unconventional approaches [9–14] are also used. However, to the best of our knowledge, there are few studies focused on optimizing the linear designs of a cell [1, 2], and no established protocols specifically address this type of optimization without relying on typical nonlinear functions, such as dynamic aperture.

Recently, polynomial quasi-invariants of motion [15–18] have been employed to optimize the nonlinear design of a fourth-generation synchrotron light source storage ring [19]. This approach eliminates the need for particle tracking calculations, thereby reducing the reliance on costly computational resources. Here, we propose a framework that extend this approach to optimize the linear parameters of a lattice without requiring particle tracking or other similar nonlinear calculations. This framework utilizes the distorted chromatic index $\zeta_{D,\delta}$, a valuable tool for analyzing and tuning a cell to identify a suitable working point for a machine. As an example, this technique is used to identify a working point for a ring model based on a 7BA cell, which consists of 20 cells and has a circumference of approximately 490 meters. Following nonlinear optimization, this approach enhances the horizontal dynamics of the ring.

* esanchez@icf.unam.mx

THE METHOD

The work in Ref. [6] demonstrates that a storage ring can be modeled using a two-dimensional nonlinear Hamiltonian that incorporates chromatic effects

$$H(x,p_x,y,p_y,s) = \frac{1}{2}(p_x^2+p_y^2)\left(1-\delta+\delta^2+\cdots\right) - b_1(s)\,x\,\delta + \frac{b_1^2(s)}{2}x^2 + \frac{b_2(s)}{2}\left(x^2-y^2\right) + \frac{b_3(s)}{3}\left(x^3 - 3xy^2\right) + \frac{b_4(s)}{4}\left(x^4-6x^2y^2+y^4\right)+\cdots, \quad (1)$$

where the functions $b_1(s)$, $b_2(s)$, $b_3(s)$, and $b_4(s)$, are related to the magnetic field derivatives, and $\delta = \frac{\Delta p}{p_0}$ is the percentage deviation from the momentum p_0. A quasi-invariant polynomial surface [18, 19] can be associated with this system. Up to order δ^2, it can be written as follows

$$S(x,p_x,y,p_y,\delta) = \sigma_1 + \sigma_{\rm nl} + \sigma_{\delta^1}\,\delta + \sigma_{\delta^2}\,\delta^2, \quad (2)$$

with σ_1, $\sigma_{\rm nl}$, σ_{δ^1} and σ_{δ^2} its non-chromatic linear, non-chromatic nonlinear, first-order chromatic and second-order chromatic contributions, respectively.

After substituting Eq. (2) into the invariance condition

$$\frac{d}{ds}S = \{S,H\} + \frac{\partial}{\partial s}S = 0, \quad (3)$$

ISBN: 978-3-95450-219-6 ISSN: 2226-0366 doi: 10.18429/JACoW-LINAC2024-THPB096

the following equations are derived for various powers of δ

$$\delta^{(0)}: \frac{\partial}{\partial s}\sigma_1 + \{\sigma_1, H_1\} = 0, \tag{4a}$$

$$\frac{\partial}{\partial s}\sigma_{\rm nl} + \{\sigma_{\rm nl}, H_1 + V_{\rm nl}\} = -\{\sigma_1, V_{\rm nl}\}, \tag{4b}$$

$$\delta^{(1)}: \frac{\partial}{\partial s}\sigma_{\delta^1} + \{\sigma_{\delta^1}, H_1 + V_{\rm nl}\} = -\{\sigma_1, V_{\delta^1}\} - \{\sigma_{\rm nl}, V_{\delta^1}\}, \tag{4c}$$

$$\delta^{(2)}: \frac{\partial}{\partial s}\sigma_{\delta^2} + \{\sigma_{\delta^2}, H_1 + V_{\rm nl}\} = -\{\sigma_1, V_{\delta^2}\} - \{\sigma_{\rm nl}, V_{\delta^2}\} - \{\sigma_{\delta^1}, V_{\delta^1}\}. \tag{4d}$$

where

$$H_1 = H_0 + \frac{1}{2}\left(p_y^2 - b_2(s)\, y^2\right), \tag{5a}$$

$$V_{\rm nl} = \frac{b_3(s)}{3}\left(x^3 - 3xy^2\right) + \frac{b_4(s)}{4}\left(x^4 - 6x^2y^2 + y^4\right), \tag{5b}$$

$$V_{\delta^1} = -\frac{1}{2}(p_x^2 + p_y^2) - b_1(s)\, x, \tag{5c}$$

$$V_{\delta^2} = \frac{1}{2}(p_x^2 + p_y^2), \tag{5d}$$

represent the contributions to the dynamics from linear, nonlinear, first-order chromatic, and second-order chromatic effects, respectively.

In this study, the surface Eq. (2) is represented by a polynomial of degree 8, up to first-order in δ. This resulted in a system of 418 coupled ordinary differential equations, which were manipulated using wxMaxima [20]. Details of this process can be found in Ref. [19].

Only the projected surfaces (Eq. (2)) in horizontal phase space (with $y = 0$ and $p_y = 0$)) are analyzed. To generate the 3-D surfaces graphs, the *surf* function in MATLAB® was used. To create 2-D contour lines, the *contour* function from the same environment was utilized. Additionally, the simulations presented in this investigation were obtained using the OPA particle tracking module [21].

In general, an appropriate choice of magnetic functions b_n facilitates the quasi-integrability of the system (Eq. (1)), which is related to the deformation of the surface (Eq. (2)). Figure 1 displays a representative quasi-invariant surface, with $y = 0$ and $p_y = 0$, associated with the considered ring.

It is well-established that properly arranged families of chromatic sextupoles can reduce the strength of nonlinear resonances (see, for example, Ref. [22]). This study proposes that the distortion introduced by these sextupole families in the surfaces $S_{D,\delta}$, which are associated with a Hamiltonian (Eq. (1)) that includes only the nonlinear effects of the sextupoles, provides crucial information about the resonances in a given system (defined by specific linear parameters). The main hypothesis is that as the surfaces $S_{D,\delta}$ approach the reference surface S_0, which corresponds to the linear approximation of the Hamiltonian (Eq. (1)) [18], the effects of nonlinearities will be minimized.

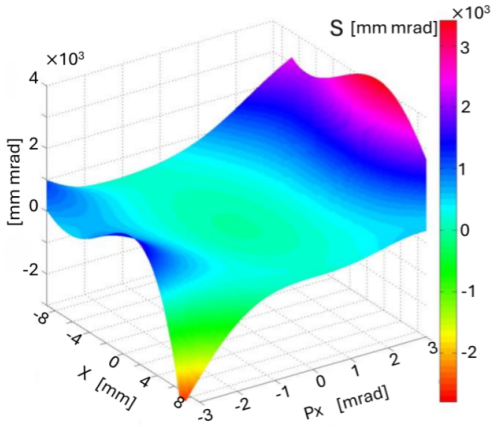

Figure 1: A representative quasi-invariant surface, with $y = 0$ and $p_y = 0$, associated with the considered ring. The observed distortion is due to nonlinearities.

The difference between the surfaces surfaces $S_{D,\delta}$ and the reference surfaces S_0 [18] is defined as follows

$$X_{D,\delta} \equiv X(S_{D,\delta}) = \sum_{j=1}^{N}\sum_{i=1}^{N} |S_{D,\delta}(x_i, p_j) - S_0(x_i, p_j)|, \tag{6}$$

where a uniform mesh of dimension $N \times N$ ($N = 80$), centered at the origin and defined for a maximum oscillation amplitude x_0, was used. The values of the surfaces $S_{D,\delta}$ and S_0 were calculated at the vertices of this mesh.

It is useful to estimate the distortion in N_δ phase spaces with δ in the interval (δ_m, δ_M). Using the distribution of values $\{X_{D,\delta}\}$, several functions were calculated: the mean

$$\mu = \frac{1}{N_\delta}\sum_{\delta=\delta_m}^{\delta_M} X_{D,\delta}, \tag{7}$$

which represents the average of the distribution of differences (Eq. (6)); the standard deviation

$$\Sigma = \sqrt{\frac{1}{N_\delta - 1}\sum_{\delta=\delta_m}^{\delta_M} |X_{D,\delta} - \mu|^2}, \tag{8}$$

which measures the variation of these differences (Eq. (6)) with respect to the mean; and the skewness

$$s = \frac{1}{N_\delta \Sigma^2}\sum_{\delta=\delta_m}^{\delta_M} (X_{D,\delta} - \mu)^3, \tag{9}$$

which assesses the asymmetry of the distribution of differences (Eq. (6)).

Equations (6)-(9) are used to define the *distorted chromatic index*

$$\zeta_{D,\delta} \equiv= \sqrt{\mu^2 + \Sigma^2 + s^2}. \tag{10}$$

This index, given by Eq. (10), depends directly on the linear parameter configuration of the ring and measures the degree of dissimilarity between the set $\{X_{D,\delta}\}$ and the reference surface S_0.

ISBN: 978-3-95450-219-6 ISSN: 2226-0366 doi: 10.18429/JACoW-LINAC2024-THPB096

RESULTS

A storage ring model based on the MBA cells from the ESRF-EBS [23] and SLS-2 [24] synchrotrons, and utilized in Ref. [19], was employed in this application. The main parameters of this model are listed in Table 1.

Table 1: Main storage ring parameters considered.

Parameter	Value
Type of superperiod	7BA
Energy	3 GeV
Cells	20
Number of free-space lengths varied	3
Number of quadrupole strengths varied	6

Figure 2 illustrates the working points for 50,000 variants of this ring model. These variants were randomly generated by varying linear parameters such as quadrupole magnetic strengths and free space distances. All variants satisfy stability conditions and the usual constraints on the values of linear optical functions. The color assigned to each tune represents the value of the distorted chromatic index $\zeta_{D,\delta}$, calculated for $N_\delta = 250$ equidistant values of δ ranging from $\delta_m = -1\%$ to $\delta_M = 1\%$.

As shown in Fig. 2, varying parameters of the ring allows for the representation of resonance structures in tune space, based on the information provided by the distorted chromatic index $\zeta_{D,\delta}$.

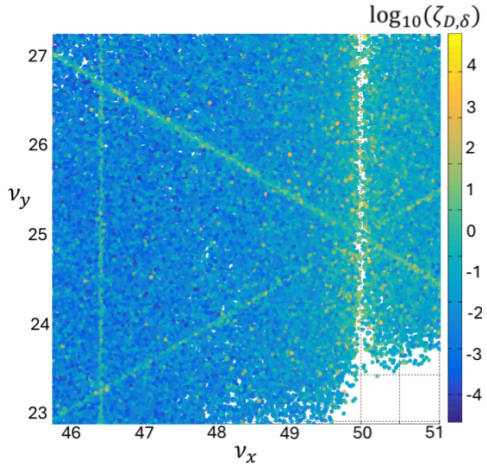

Figure 2: Tunes of variants of the considered ring; color corresponds to the distorted chromatic index value $\zeta_{D,\delta}$ for the respective linear parameter configuration.

Linear Tuning

Linear parameters of the ring model were varied to minimized the index (Eq. (10)). Throughout this process, stability conditions and standard constraints on the values of linear optical functions were met. The final linear configuration of the model results in a storage ring with the parameters shown in Table 2.

Table 2: Main storage ring parameters considered after minimization of the distorted chromatic index.

Parameter	Value
Circumference (m)	486.51 m
Betatron tunes (ν_x, ν_y)	48.44, 26.88
Natural chromaticity (ξ_x, ξ_y)	−80.62, −59.21
Emittance	81 pm rad

Nonlinear Optimization

Nonlinear optimization [19] was applied to both the non-optimized and final linear configurations of the ring. For the optimized linear configuration, stable amplitudes exceeding 5 mm were achieved for momentum deviations between −3% and 3%. Figure 3 shows how the horizontal stability region improves when the index (10) is minimized.

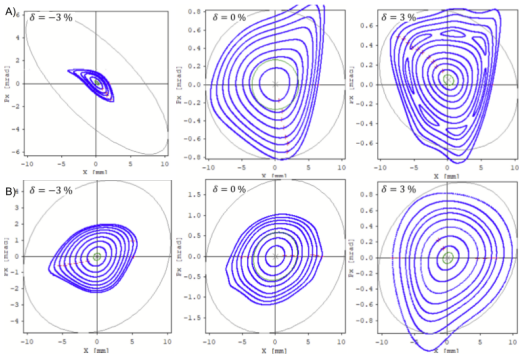

Figure 3: A) Horizontal stability regions without using the distorted chromatic index; B) horizontal stability regions when distorted chromatic index was minimized. Equivalent nonlinear optimizations were performed in both cases.

CONCLUDING REMARKS

The order, type and specific width of resonances that can be observed in tune diagrams using this method depend on the model studied.

Minimizing the distorted chromatic index enables the selection of a specific lattice configuration and its corresponding working point.

After minimizing the distorted chromatic index, nonlinear optimization resulted in stable amplitudes exceeding 5 mm for momentum deviations ranging from −3% to 3%.

Although the horizontal stability regions have been improved, the dynamic aperture has not been fully optimized. This issue could be addressed by incorporating vertical effects in the selection of the optimal working point. Efforts are underway to explore this approach.

ACKNOWLEDGEMENTS

This work was supported by UNAM-PAPIIT IN108522. Proyecto apoyado por el “CONACYT” en el año 2023, with number CF-2023-I-119. E.A.S. is grateful to CONACYT for funding a postdoctoral fellowship.

ISBN: 978-3-95450-219-6 ISSN: 2226-0366 doi: 10.18429/JACoW-LINAC2024-THPB096

REFERENCES

[1] D. S. Robin, W. Wan, F. Sannibale, and V. P. Suller, "Global analysis of all linear stable settings of a storage ring lattice", *Phys. Rev. Spec. Top. Accel. Beams*, vol. 11, p. 024 002, 2008. doi:10.1103/PhysRevSTAB.11.024002

[2] L. Yang, D. Robin, F. Sannibale, C. Steier, and W. Wan, "Global optimization of an accelerator lattice using multiobjective genetic algorithms", *Nucl. Instrum. Methods Phys. Res., Sect. A*, vol. 609, no. 1, pp. 50–57, 2009.

[3] Y. Papaphilippou, "Detecting chaos in particle accelerators through the frequency map analysis method", *Chaos*, vol. 24, no. 2, p. 024 412, 2014. doi:10.1063/1.4884495

[4] J. Irwin, "The application of lie algebra techniques to beam transport design", *Nucl. Instrum. Methods Phys. Res., Sect. A*, vol. 298, no. 1-3, pp. 460–472, 1990.

[5] W. Gao, L. Wang, and W. Li, "Simultaneous optimization of beam emittance and dynamic aperture for electron storage ring using genetic algorithm", *Phys. Rev. Spec. Top. Accel. Beams*, vol. 14, no. 9, p. 094 001, 2011. doi:10.1103/PhysRevSTAB.14.094001

[6] J. Bengtsson, "The Sextupole Scheme for the Swiss Light Source (SLS): An Analytical Approach", Paul Scherrer Institute, Villigen, Switzerland, 1997. https://ados.web.psi.ch/slsnotes/sls0997.pdf

[7] Y. Li and L. Yang, "Multi-objective dynamic aperture optimization for storage rings", *Int. J. Mod. Phys. A*, vol. 31, no. 33, p. 1 644 019, 2016. doi:10.1142/S0217751X1644019X

[8] B. Wei, Z. Bai, J. Tan, L. Wang, and G. Feng, "Minimizing the fluctuation of resonance driving terms in dynamic aperture optimization", *Phys. Rev. Spec. Top. Accel. Beams*, vol. 26, no. 8, p. 084 001, 2023.

[9] M. Kranjčević, B. Riemann, A. Adelmann, and A. Streun, "Multiobjective optimization of the dynamic aperture using surrogate models based on artificial neural networks", *Phys. Rev. Spec. Top. Accel. Beams*, vol. 24, no. 1, p. 014 601, 2021. doi:10.1103/PhysRevAccelBeams.24.014601

[10] Y. Li, K. Hwang, C. Mitchell, R. Rainer, R. Ryne, and V. Smaluk, "Design of double-bend and multibend achromat lattices with large dynamic aperture and approximate invariants", *Phys. Rev. Spec. Top. Accel. Beams*, vol. 24, p. 124 001, 2021.

[11] Y. Lu *et al.*, "Enhancing the MOGA Optimization Process at ALS-U with Machine Learning", in *Proc. IPAC'21*, Campinas, Brazil. May 2021 (online), pp. 387–390. doi:10.18429/JACoW-IPAC2021-MOPAB106

[12] Y. Li, Y. Hao, K. Hwang, R. Rainer, A. He, and A. Liu, "Fast dynamic aperture optimization with forward-reversal integration", *Nucl. Instrum. Methods Phys. Res., Sect. A*, vol. 988, p. 164 936, 2021.

[13] J. Wan and Y. Jiao, "Machine learning enabled fast evaluation of dynamic aperture for storage ring accelerators", *New J. Phys.*, vol. 24, no. 6, p. 063 030, 2022.

[14] Y. Lu *et al.*, "Demonstration of machine learning-enhanced multi-objective optimization of ultrahigh-brightness lattices for 4th-generation synchrotron light sources", *Nucl. Instrum. Methods Phys. Res., Sect. A*, vol. 1050, p. 168 192, 2023.

[15] A. Antillón, "Emittance for a nonlinear machine: The one-dimensional problem", *Part. Accel.*, vol. 23, pp. 187–195, 1988.

[16] A. Antillon, E. Forest, B. Hoeneisen, and F. Leyvraz, "Transport matrices for nonlinear lattice functions", *Nucl. Instrum. Methods Phys. Res., Sect. A*, vol. 305, no. 2, pp. 247–256, 1991.

[17] A. Antillón and B. Hoeneisen, "Emittance of a nonlinear machine: The two-dimensional problem", *Nucl. Instrum. Methods Phys. Res., Sect. A*, vol. 305, no. 2, pp. 239–246, 1991.

[18] E. A. Sánchez, A. Flores, J. Hernández-Cobos, M. Moreno, and A. Antillón, "Increasing beam stability zone in synchrotron light sources using polynomial quasi-invariants", *Sci. Rep.*, vol. 13, no. 1, p. 1335, 2023.

[19] E. A. Sanchez, A. Flores, J. Hernandez-Cobos, M. Moreno, and A. Antillón, "A novel approach using nonlinear surfaces for dynamic aperture optimization in mba synchrotron light sources", *Sci. Rep.*, vol. 13, no. 1, p. 23 007, 2023.

[20] *wxMaxima, version 22.03.0*, 2022. https://sourceforge.net/projects/wxmaxima/

[21] A. Streun, "OPA, Lattice Design Code". https://ados.web.psi.ch/opa/

[22] H. Wiedemann, *Particle Accelerator Physics*. Springer Nature, 2015.

[23] S. M. White *et al.*, "Commissioning and Restart of ESRF-EBS", in *Proc. IPAC'21*, Campinas, Brazil, May 2021 (online), pp. 1–6. doi:10.18429/JACoW-IPAC2021-MOXA01

[24] A. Streun *et al.*, "SLS-2–the upgrade of the swiss light source", *J. Synchrotron Radiat.*, vol. 25, no. 3, pp. 631–641, 2018. doi:10.1107/S1600577518002722